In Vivo Imaging of the Human Retinal Pigment Epithelial Mosaic Using Adaptive Optics Enhanced Indocyanine Green Ophthalmoscopy

Johnny Tam,[1] Jianfei Liu,[1] Alfredo Dubra,[2–4] and Robert Fariss[5]

[1]Ophthalmic Genetics and Visual Function Branch, National Eye Institute, National Institutes of Health, Bethesda, Maryland, United States
[2]Department of Ophthalmology, Medical College of Wisconsin, Milwaukee, Wisconsin, United States
[3]Department of Biophysics, Medical College of Wisconsin, Milwaukee, Wisconsin, United States
[4]Department of Cell Biology, Neurobiology, and Anatomy, Medical College of Wisconsin, Milwaukee, Wisconsin, United States
[5]Biological Imaging Core, National Eye Institute, National Institutes of Health, Bethesda, Maryland, United States

PURPOSE. The purpose of this study was to establish that retinal pigment epithelial (RPE) cells take up indocyanine green (ICG) dye following systemic injection and that adaptive optics enhanced indocyanine green ophthalmoscopy (AO-ICG) enables direct visualization of the RPE mosaic in the living human eye.

METHODS. A customized adaptive optics scanning light ophthalmoscope (AOSLO) was used to acquire high-resolution retinal fluorescence images of residual ICG dye in human subjects after intravenous injection at the standard clinical dose. Simultaneously, multimodal AOSLO images were also acquired, which included confocal reflectance, nonconfocal split detection, and darkfield. Imaging was performed in 6 eyes of three healthy subjects with no history of ocular or systemic diseases. In addition, histologic studies in mice were carried out.

RESULTS. The AO-ICG channel successfully resolved individual RPE cells in human subjects at various time points, including 20 minutes and 2 hours after dye administration. Adaptive optics-ICG images of RPE revealed detail which could be correlated with AO dark-field images of the same cells. Interestingly, there was a marked heterogeneity in the fluorescence of individual RPE cells. Confirmatory histologic studies in mice corroborated the specific uptake of ICG by the RPE layer at a late time point after systemic ICG injection.

CONCLUSIONS. Adaptive optics-enhanced imaging of ICG dye provides a novel way to visualize and assess the RPE mosaic in the living human eye alongside images of the overlying photoreceptors and other cells.

Keywords: adaptive optics, indocyanine green, ophthalmoscopy, retinal imaging, retinal pigment epithelium

Indocyanine green (ICG) dye is an extrinsic fluorophore routinely used to image the retinal and choroidal vasculature and is excited using infrared light.[1,2] Its rapid clearance from the blood after initial intravenous injection (half-life of a few minutes) establishes a time window of approximately 30 minutes, after which it is thought that little or no additional clinically useful information can be derived. In fact, the later phases of ICG imaging (beyond 30 minutes after administration) remain relatively unexplored. One study reported a residual ICG signal in patients' eyes 24 hours post injection.[3] At that time-point, in the absence of vascular signal, well-demarcated hypofluorescent lesions were described in patients with age-related macular degeneration. Notably, in both healthy eyes and nonlesion areas of diseased eyes, a weak, but visible ICG signal was still visible. The source of this signal remains to be determined. Histologic evidence has suggested that there may be accumulation of ICG dye in the late phase within retinal pigment epithelial (RPE) cells.[4,5] To explore this phenomenon, we further investigated whether ICG could be used for imaging the RPE cells in the living human eye with adaptive optics (AO) ophthalmoscopy.

Adaptive optics ophthalmoscopy provides new opportunities for imaging the retinal tissue at a resolution that is sufficient for visualizing individual cells.[6–11] Although some retinal cells, such as photoreceptors, have intrinsic single or multiple scattering contrast and can be readily imaged,[7–9,11] other cells have little or no signal and therefore require different strategies for their successful visualization, such as the use of AO optical coherence tomography (OCT).[12–14] In general, the RPE cells cannot be routinely imaged using AO confocal reflectance imaging, except when the overlying photoreceptors are absent.[15] Single-photon ophthalmic AO autofluorescence imaging has been used to visualize the RPE mosaic, based on the use of visible wavelengths of light to excite lipofuscin within these cells.[16] Due to concerns related to the risk of phototoxicity associated with visible wavelengths used in this technique,[17,18] careful adherence to stringent limits of light exposure is required, and automated focusing or real-time eye tracking may also be required.[19,20] Adaptive optics 2-photon fluorescent

imaging of the RPE mosaic is also possible in animals but currently only with light levels that are above maximum permissible exposure limits.[21] Recently, AO dark-field images of RPE were generated.[22] However, in our hands, this technique is successful in only a small minority of individuals, and when successful, it is only able to visualize RPE cells in the fovea.

Adaptive optics ophthalmoscopes can be modified for single-photon fluorescence by adding an excitation light source and appropriate emission filters, as was demonstrated for imaging the passage of fluorescein dye through the retinal vasculature.[23,24] In a similar manner, we modified our AO ophthalmoscope to detect near-infrared fluorescence light for imaging of ICG, which we then used to demonstrate a novel approach for imaging individual RPE cells in the living human eye. In our particular instrument, we simultaneously captured confocal reflectance images of photoreceptors,[10] split detection images of photoreceptor inner segments,[25] dark-field images of RPE cells,[16] and single-photon near-infrared fluorescence images of RPE cells. Our late-phase AO-ICG images alongside confirmatory histologic studies in mice establish that RPE cells contribute to the fluorescence signal observed in the late phase of ICG.

METHODS

Human Subjects

Research procedures adhered to the tenets of the Declaration of Helsinki. Written informed consent was obtained after the nature of the research and possible consequences of the study were explained. The study was approved by the Institutional Review Board of the National Institutes of Health. Three healthy volunteers with no history of systemic or ocular disease were recruited to undergo AO-ICG imaging in both eyes. Prior to imaging, eyes were dilated with 1 drop of 2.5% phenylephrine hydrochloride and 1 drop of 1% tropicamide.

AO Instrumentation

A replica of a broadband adaptive optics scanning light ophthalmoscope (AOSLO) was assembled as described previously.[10] In addition, split detection and dark-field imaging capabilities were added.[22,25] Wavefront sensing was performed using an 850 nm light source, and imaging was performed using a broadband (~17 nm full width at half maximum) 790 nm light source with a beam diameter of 7.75 mm at the point of entry into the eye. This system was further modified to enable the excitation and detection of ICG fluorescence. Specifically, an additional photomultiplier tube capable of near-infrared detection was added for ICG imaging (product H7422A-50; Hamamatsu, Shizuoka, Japan), along with a dichroic filter (product LPD02-830RU-25; Semrock, Rochester, NY, USA), and two additional filters in front of the detector (products FF01-842/SP and FF01-832/37; Semrock) to effectively collect light between 810 and 830 nm. A pinhole with a 3 Airy-disk diameter was used. A bandpass filter was placed in front of the 790 nm light source to restrict the excitation wavelengths to only those wavelengths below 800 nm (product ET775/50X; Chroma Technology, Bellow Falls, VT, USA), as well as in front of the 850 nm light source to prevent light less than 840 nm from reaching the eye (product FF01-850/10; Semrock). These additional filters slightly reduced the power of the light as measured at the cornea. Imaging was performed using either a 90/10 or an 80/20 (% Transmission/ % Reflection) system beam splitter. In this study, the light power levels measured at the cornea were maintained below 100 μW for the 790 nm source and 35 μW for the 850 nm

source, which are under the maximum permissible exposure set by American National Standards Institute standard Z136.1 2014.[26]

AO Imaging

Twenty- to 30-second videos were acquired at various retinal locations at an imaging rate of 17 frames per second. The locations were selected with some overlap, using square field sizes ranging from 0.75° to 2.0° and included the fovea and parafoveal regions of both eyes, both prior to and after ICG injection. Additional peripheral regions were also selected for imaging at 5°, 10°, and 15° eccentricity in the temporal direction. Indocyanine green was administered intravenously as a single bolus at a dose of 25 mg in 3 mL, according to the standard of care at the National Eye Institute Eye Clinic. During each recording, four image sequences were acquired simultaneously: AO confocal reflectance, ICG fluorescence (AO-ICG), and two additional channels containing multiple scattered light from opposing directions of the confocal detector, which were used to generate AO split detection and AO dark-field images. In total, 1984 videos were acquired over six separate imaging sessions. A computer-controlled fixation system was used to facilitate the capture of images.[19] During imaging, the focal plane was set to that of the photoreceptors based on a previous report stating that the optimal focal plane for AO dark-field RPE imaging was the plane of optimal photoreceptor imaging.[22] Biometry measurements were also acquired from all subjects (IOL Master; Carl Zeiss Meditec, Dublin, CA, USA) and used to determine scaling factors to convert pixels to micrometers.

AO Image Processing

Videos were postprocessed to correct for eye motion, using customized software, as described previously.[27] Because four videos were acquired simultaneously, the video with the (subjectively determined) sharpest features was selected for the computation of eye motion, which in all cases was the AO confocal reflectance channel. The computed eye motion was then applied to the other three corresponding videos,[16] which enabled accurate registration of even those videos with little or no signal (e.g., ICG videos acquired prior to the injection of ICG dye can be registered using this strategy). After eye motion correction, registered frames were averaged, and a montage was manually created using Photoshop software (Adobe, San Jose, CA, USA). With the exception of quantitative analyses described below, the maximum number of successfully registered frames was included for averaging (up to a total of 500 possible frames). For display purposes, AO-ICG and AO dark-field image contrast ranges were stretched between the minimum and maximum values.

Quantitative Analysis

A subset of human AO-ICG data was selected for further analysis. For each subject, a 0.9° square region of interest that showed the clearest RPE cell outlines on the AO dark-field images was selected for further analysis. Using ImageJ software (ImageJ, US National Institutes of Health, Bethesda, MD, USA; available in the public domain, http://imagej.nih.gov/ij/), we manually identified the centers of RPE cells based on the locations of cell outlines and following the assumption that RPE cells form a uniform hexagonal array in healthy volunteers. These cell centers were then used to construct Voronoi neighborhoods[28] to facilitate qualitative comparisons between AO dark-field and AO-ICG images in order to determine whether there was a correspondence between the cell outlines

seen using AO dark-field and the pattern seen using AO-ICG. In addition, cell density was computed by dividing the number of identified cell centers by the area of the region of interest and compared to previously published values of RPE cell density based on histology.

Relative intensity measurements were also carried out to verify the uptake of ICG dye. In human subjects, fluorescence intensity values were measured from raw data as the average across a single video acquired at the fovea both prior to the injection of ICG and 2 hours afterward (acquisition parameters were kept constant for this analysis: 1.5° field of view, 200 frames acquired at 17 Hz, ICG photomultiplier tube gain setting of 0.500, focus set to the plane of best photoreceptor focus). The preinjection video was used as the baseline intensity, and the relative intensity was calculated by dividing the mean of the postinjection site video by the mean of the preinjection video in order to derive an estimate of the signal strength. For mouse data (described below), the average intensity value of the image acquired in the ICG channel was measured by drawing a line through the RPE layer and taking the average of the intensity values along the line, using ImageJ software. In this case the relative intensity was computed by dividing the measured intensities in an injected mouse by those in a noninjected mouse. Human data were paired before and after injection, and mice data were paired by siblings (injected and noninjected). A 1-tailed paired *t*-test was used to evaluate whether ICG injection resulted in an increase in detected fluorescence intensity.

Experimental Animals

Experiments were conducted according to protocols approved by a local Institutional Animal Care and Use committee and in compliance with the ARVO Statement for the Use of Animals in Ophthalmic and Vision Research. All animals were housed and bred in the National Institutes of Health animal facilities. Ten mice from various backgrounds were used (6 C57BL/6J, 2 B6-albino, 2 OTO2-10). Mice were paired into five sets of 2 siblings with each pair taken from the same litter. The age of the mice ranged from 2 to 6 months (average, 3.5 months). Intraperitoneal injection of ICG was performed in one mouse from each pair (200 μL of 5 mg/mL solution).

Histology

Experimental animals were euthanized by carbon dioxide inhalation at a 16 hours after administration of ICG dye for the ICG-injected mice. Immediately after enucleation, eyes were embedded in optical cutting temperature (OCT) compound and rapidly frozen using acetone, cooled to approximately −70°C by addition of dry ice. No fixation agents were used based on our own experience and prior reports that ICG localization within the ocular tissue is altered due to the highly soluble nature of ICG.[4] Cryosections (8–10 μm) were cut through the center of the eye, collected on Super-frost Plus microscope slides (Fisher Scientific, Waltham, MA, USA), vacuum dried, and mounted in Immu-Mount (ThermoFisher Scientific, Rockville, MD, USA).

Microscopy

To prevent diffusion of ICG dye into the unfixed tissue, cryosections were imaged immediately after mounting. Microscopy was performed using a modified Axio imager Z1 microscope (Carl Zeiss) outfitted with an X-Cite 200DC light source (Lumen Dynamics, Mississauga, ON, Canada) and an ICG filter kit (product ICG-B-ZHE-ZERO; Semrock), which enabled near-infrared imaging of ICG. All ICG images were acquired using a 1.30 numerical aperture 40× objective and AxioCam MRm charge-coupled device camera (Carl Zeiss) with an exposure of 4.0 seconds. Autofluorescence images of cryosections were acquired sequentially (immediately after ICG imaging) to allow for the identification of retinal layers (450–490 nm excitation, 500–550 nm detection).

RESULTS

Following systemic injection of ICG into three human subjects (HV1: 33-year-old male; HV2: 40-year-old female; HV3: 25-year-old female), a heterogeneous AO-ICG signal was observed by using the modified AOSLO that was qualitatively distinct from both AO confocal reflectance and AO dark-field images of the same retinal region (Fig. 1). Whereas only cell outlines were visible under AO dark-field illumination, entire cells appeared to be visible using AO-ICG. The structures visible on AO-ICG imaging were hexagonal in appearance and several-fold larger in size than cone photoreceptors, consistent with the expected size of RPE cells.

Adaptive optics dark-field imaging was used to confirm that these cells were indeed RPE cells. In regions where individual RPE cells could be visualized using both AO dark-field imaging and AO-ICG imaging, there was good correspondence between the two techniques (Fig. 2). A total of 2,209 RPE cells were manually identified in 3 regions of interest (ROI) near the fovea of three eyes (approximate eccentricity of the center of each ROI was 1.1° in HVI; 1.0 in HV2; and 1.4 in HV3; each ROI was 1.5°). The density of the RPE cells based on manual cell labeling (Fig. 2) was 5488, 6564, and 5382 cells/mm^2 for the three subjects (average: 5811 cells/mm^2), comparable to a previously published report of RPE cell density in humans[29] (7500 cells/mm^2 peak density at fovea, decreasing to 5000 cells/mm^2 at an approximate eccentricity of 1°) and in monkeys[16] (5260 ± 320 cells/mm^2 peak density at fovea, decreasing to 5110 ± 310 cells/mm^2 at 1°). Voronoi neighborhoods generated from the manually identified cells overlapped with the individual patterns seen in AO-ICG, suggesting that ICG accumulates in the cytoplasm of RPE cells.

The axial resolution of confocal scanning systems is poor relative to its lateral resolution when imaging using the AOSLO in the human eye. Hence, histology of mouse eyes was used to confirm the layer-specific localization of the dye following systemic injection. In all cases, there was an increase in ICG fluorescence signal that was specific to the RPE layer following systemic ICG injection (Fig. 3D). Measurements of fluorescence within the RPE layer were higher in the ICG-injected animals than in their noninjected siblings, with an average intensity increase of 4.7-fold. This intensity increase was statistically significant ($P < 0.05$). The example shown in Figure 3 illustrates a 2.7-fold increase in intensity from one pair of C57BL6/J mice. No ICG fluorescence was detected in the inner retina. In humans, from in vivo adaptive optics imaging data, there was an average 2.5-fold increase in intensity, comparing intensity values 2 hours after injection to the same area prior to injection ($P < 0.05$). Prior to injection, there was no detectable signal (e.g., no leakage of excitation or wavefront sensing light into the AO-ICG detection channel) (Fig. 4).

The AO-ICG signal was robust across all imaging parameters that were tried. Although the RPE mosaic was not visible on a single frame, it was easily visible after accumulation of as few as 10 frames, corresponding to approximately 400 ms of cumulative light exposure (Fig. 4). We tested two different beam splitters to couple the light sources (10% or 20% reflection) and the detectors (90% or 80% transmission, respectively). The use of an 80/20 beam splitter (HV2 and
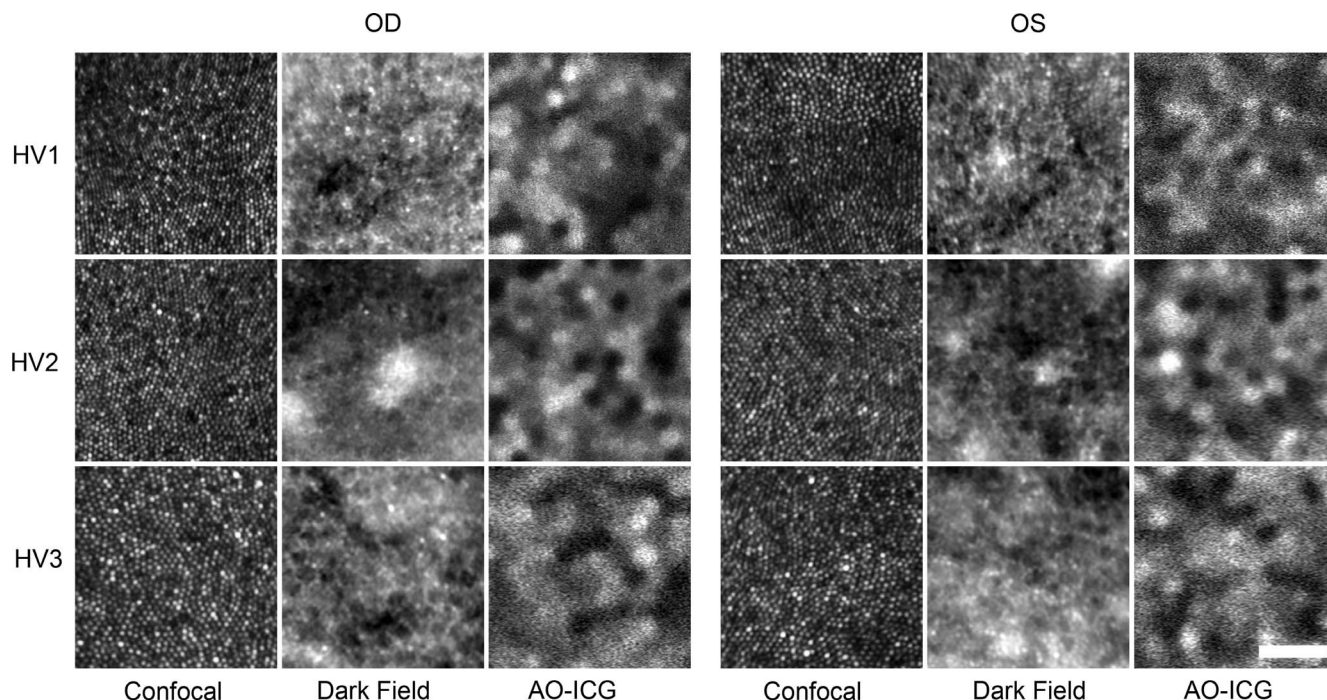
FIGURE 1. Three different modes of adaptive optics retinal images captured simultaneously in the foveas of three human subjects (HV1, HV2, and HV3). (*Left* to *right*) Adaptive optics confocal reflectance adaptive optics image of cone photoreceptors, outlines of RPE cells revealed using darkfield AO, and near-infrared fluorescence imaging of RPE cells using AO-ICG. All ROIs were selected within 1.0° of the foveal center, which was visually identified as the area of highest cone density. *Scale bar*: 50 μm.

HV3) resulted in a similar or better AO-ICG image than that obtained using the 90/10 beam splitter (HV1), with no apparent differences in the other AO imaging modalities. AO-ICG images were nearly identical when acquired using different field sizes and even across different time points (Fig. 5). Given the longevity of this signal, and to ensure maximal clearance of ICG from the blood stream, we opted to acquire extensive AO-ICG images at the time point of 2 hours post injection (Figs. 1, 2, 4, 6, 7).

After modifying the AOSLO for ICG imaging, we were still able to simultaneously acquire high quality AO confocal reflectance and AO split-detection images alongside AO-ICG images (Fig. 6) without compromising the confocal and multiple-scattering imaging capabilities. The AO-ICG RPE signal appears to be visible over a range of retinal eccentricities within 5° of the foveal center without any noticeable drop-off in signal (Figs. 6, 7). However, at larger eccentricities, there is an imprinting effect which occurs from the overlying photoreceptors (Fig. 6).

DISCUSSION

Adaptive optics-ICG provides a novel method for imaging RPE cells within the living human eye. High-resolution single-photon fluorescence imaging revealed the presence of a stable, heterogeneous signal that persisted between 20 and 120 minutes after intravenous injection of ICG at a standard clinical dosage. This appears to be a physiologically normal phenomenon in healthy volunteers free of any signs of systemic or ocular diseases. The mechanism for this differential fluorescence remains to be explored, as it is currently unknown whether this is due to differential uptake of ICG dye or due to quenching from intrinsic pigments such as melanin, which has a broad absorption spectra that may be different in vivo than in vitro.[30] Interestingly, the heterogeneity of the prolonged ICG

signal that we observed in humans has also been reported in rats[5] and considerable cell-to-cell heterogeneity within the RPE mosaic has been shown.[31] Images of the AO-ICG signal presented in this paper will form the basis for future investigations to explore the interactions between ICG and RPE at the cellular level.

We confirmed the specific localization of ICG to the RPE cells using histologic data from mice tissue samples (Fig. 4). The selective uptake of ICG into RPE cells appears to be specific, with no substantial uptake in neighboring retinal cells. This phenomenon was robust and repeatable over a range of different mouse strains, consistent with previous reports demonstrating this phenomenon in rats[5] and nonhuman primates[4] and could be demonstrated in human subjects as shown in this paper, suggesting that it is generalizable to a potentially larger range of animal or disease models. In contrast to previous studies that administered ICG intravenously,[4,5] we administered the dye intraperitoneally in mice in order to prolong the absorption time of the dye into the RPE cells and increase the strength of the ICG signal under microscopy.

Although histologic data shows that there is instrinsic infrared autofluorescence[32,33] in the outer retina (Fig. 3B), this signal is too weak to be captured using the current implementation of AO-ICG (Fig. 4A). In mice, the ICG signal was approximately 5 times larger than the background infrared autofluorescence for pigmented mice. In support of our claim that the near infrared fluorescence in the RPE was due to injected ICG, and not due to background infrared autofluorescence, we also evaluated a pair of albino mice. Whereas the ICG fluorescence intensity in the RPE of the injected albino mouse was similar to that of the other pigmented strains, the near-infrared autofluorescence in the corresponding control (noninjected sibling) was largely undetectable. This confirms that there is uptake of ICG in the RPE following systemic injection, independent of the background infrared autofluorescence. In particular, this suggests that the background
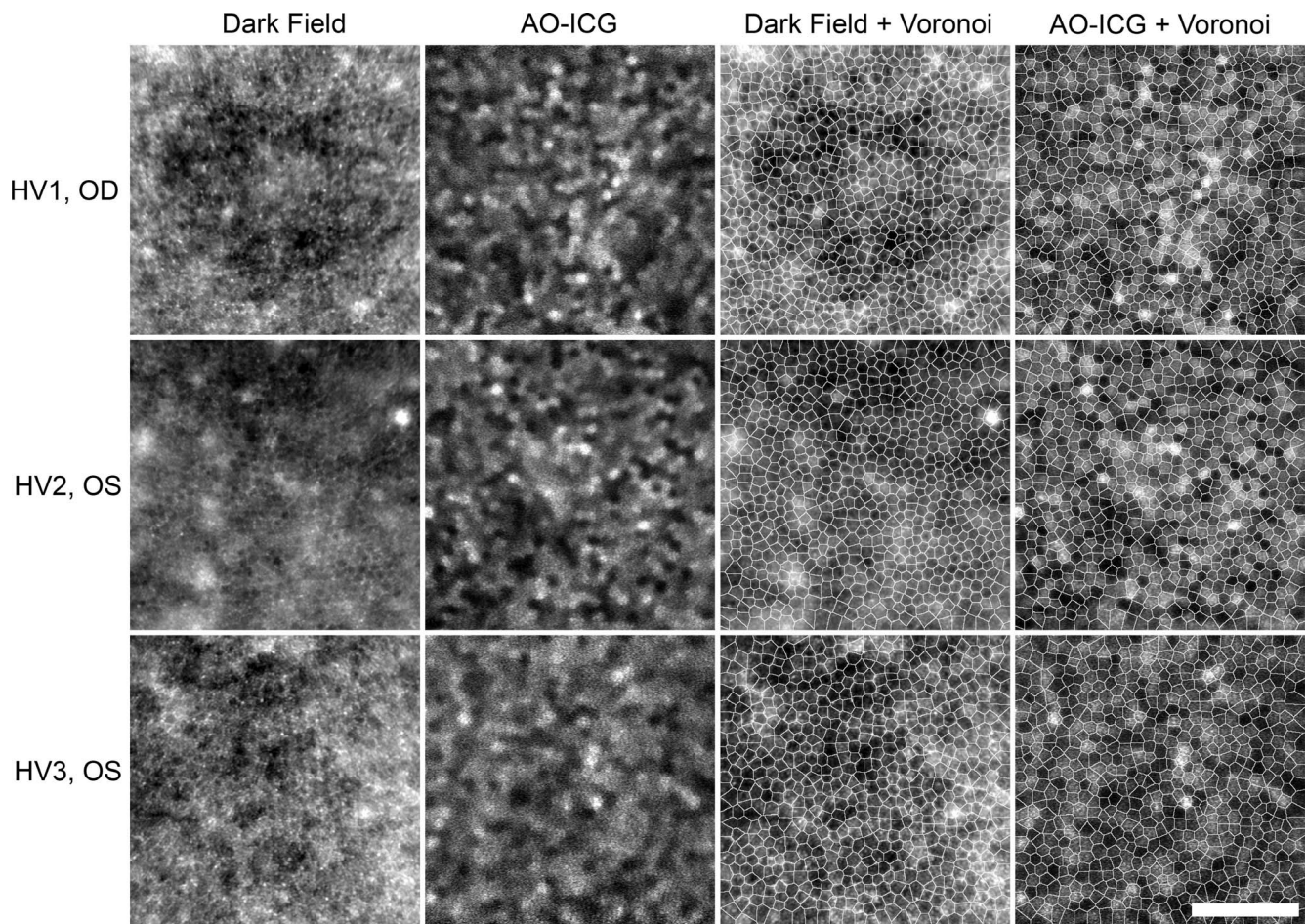
FIGURE 2. Comparison of RPE cells imaged using different ophthalmic AO modalities (one eye from each subject). (*Left* to *right*) Adaptive optics dark-field images showing cell outlines, AO-ICG fluorescence images showing entire cells, AO dark-field and AO-ICG fluorescence images with Voronoi diagrams overlaid. The Voronoi overlay was generated based on manually identified RPE cells from the dark-field image. For each subject, the same Voronoi is shown in the third and fourth columns. The ICG fluorescence within individual Voronoi neighborhoods is relatively uniform, suggesting that there is good correspondence between the cells identified using AO-DF and those using AO-ICG. *Scale bar*: 100 μm.

infrared autofluorescence signal arises largely from pigmentation (melanin) and that the strength of the ICG signal in RPE cells is many-fold higher than this background autofluorescence.

Our implementation of AO-ICG uses only one imaging light source to record four different modalities of AO images (confocal reflectance, split detection, dark field, and ICG). Because these modalities are recorded simultaneously and they originate from the same illumination source, they are in perfect registration with each other. Importantly, we have shown that the modifications that are required for AO-ICG imaging can be accomplished in a manner that does not diminish the image
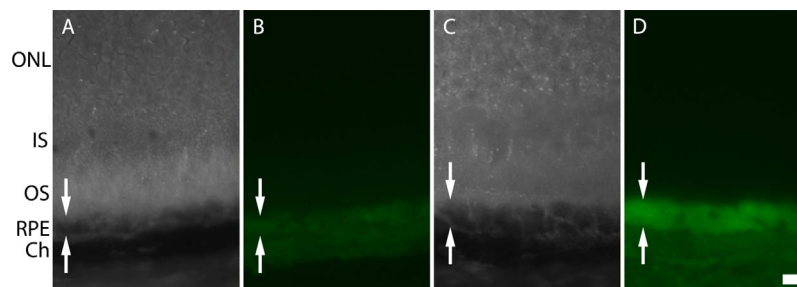

FIGURE 3. Indocyanine green imaging in a mouse eye showing that ICG dye accumulates in the RPE after systemic injection. Representative images of unfixed cryosections from an (**A, B**) noninjected mouse and (**C, D**) a mouse injected with ICG 16 hours earlier. (**A, C**) The outer retinal layers can be visualized based on the autofluorescence of the tissue. ONL, outer nuclear layer (photoreceptor nuclei); IS, photoreceptor inner segment; OS, photoreceptor outer segment; RPE, retinal pigment epithelial cells (area between *arrows*); Ch, choroid. (**B**) The RPE and choroidal layers exhibit near-infrared autofluorescence, as can be seen in the noninjected control mouse. (**D**) After ICG injection, the near-infrared fluorescence of the RPE layer is increased relative to both the noninjected mouse RPE layer and the near-infrared fluorescence. In this figure, a 2.7× increase in fluorescence signal is shown, comparing **D** to **B**. The ICG images in **B** and **D** have been increased in brightness by 4× for display purposes. *Scale bar*: 10 μm.
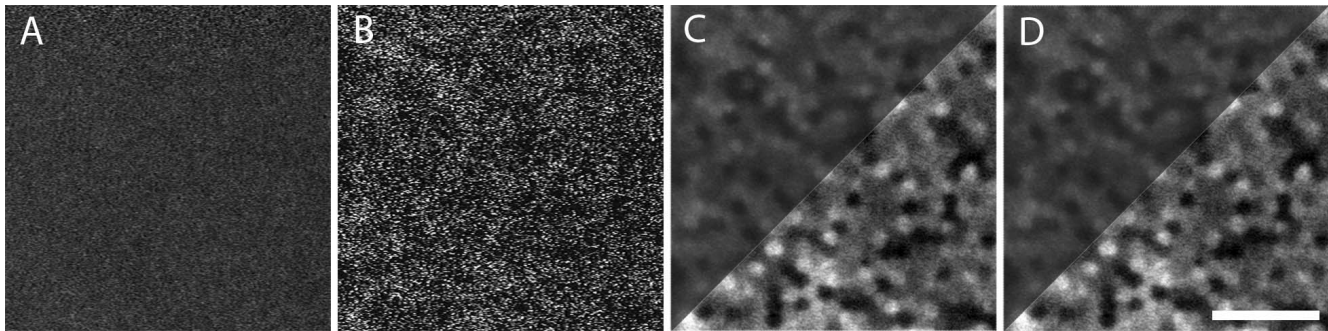
Figure 4. Illustration showing how correction of eye motion enables averaging and reconstruction of ICG signal (subject HV2, left eye). (**A**) Registered average of 300 images prior to the injection of ICG, showing no discernable signal and (**B–D**) images of the same region as **A** after injection of ICG. (**B**) Single frame (cumulative light exposure: 40 ms). A weak but discernable signal is present. (**C**) Average of 10 frames (cumulative light exposure: 400 ms). The underlying RPE structure is already visible. (**D**) Average of 100 frames (cumulative light exposure: 4 seconds). (**C**, **D**) Intensities in the *lower right half* of the image are stretched between the minimum and maximum values. All data were acquired using the same photomultiplier gain. For display purposes, a constant brightness increase of 600% was applied equally to the images shown in **A**, **B**, and *upper left halves* of **C** and **D**. *Scale bar*: 100 μm.

quality in the other channels (Figs. 1, 2, 6). The instrumentation that we used for AO dark-field imaging is an exact replica of that described in a previous paper demonstrating AO dark-field imaging of RPE cells,[22] and we were able to acquire high-quality AO dark-field images in the foveas of all three subjects. However, in our hands, AO dark-field imaging successfully revealed the RPE cells in only a small minority of subjects and is generally not successful in revealing RPE cells outside of the foveal region. Nevertheless, direct comparison between AO dark field and AO-ICG in three selected regions of interest in which AO dark field was successful established the fact that the cells visualized using AO-ICG are contained within the cell borders as seen using AO dark field. Based on a previous study, the cellular structures visualized using AO dark field also colocalize to RPE cells, revealed by AO visible-light autofluorescence imaging,[22] consistent with our observation that AO-ICG can be used to visualize RPE cells in the living human eye.

There are some important limitations of AO-ICG. First, at larger eccentricities, there is signal imprinting from overlying photoreceptors visible in the AO-ICG images (Fig. 6, the edges of the image in Fig. 7). This imprinting could represent a method with which to visualize the interaction between photoreceptors and RPE cells, as it likely arises from the excitation light being wave guided by the overlying photoreceptors.[34] Notably, whereas RPE cells could not be distinguished using AO dark-field imaging at any of the larger

eccentricities (5°, 10°, and 15°), combined color images of AO-ICG/AO split-detection suggest that with further optimization, AO-ICG may be a more robust method for imaging RPE cells outside of the fovea (Fig. 6, far right column). Second, the AO-ICG signal is weak, with an average signal increase of 2.5× after injection compared to before injection in humans. Despite the relatively weak signal, signal integration through eye motion compensation provides a reliable method for generation of images, and an AO-ICG signal can be obtained using as few as 10 frames, in the best case scenario. For comparison, the initial reports of AO autofluorescence imaging of RPE cells used between 1000 and 1700 frames.[16] Although we performed a number of optimization experiments, additional improvements in instrumentation could lead to improved signal and may also enable infrared autofluorescence imaging of RPE cells. Finally, administration of ICG dye is not without risks.[35-37] That said, the risk for adverse reactions is very low,[37] and administration of ICG dye is a standard clinical procedure and one of only a few examples of an extrinsic dye that is approved by the US Food and Drug Administration for use in the human body.[1]

Taking into consideration both the clinical and the preclinical data, we demonstrate that in the late phase of ICG imaging, RPE cells contribute to the fluorescence signal that is imaged. This finding has important implications for clinical studies. Although ICG plays a relatively limited role in the clinic in comparison to other techniques,[38] our finding
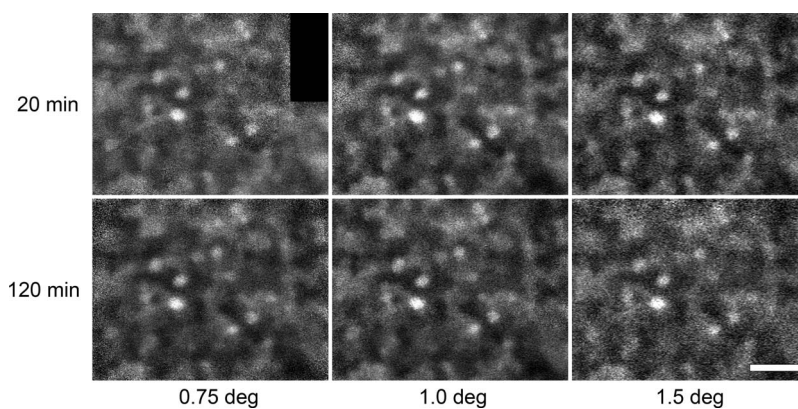

Figure 5. Imaging optimization in subject HV1, left eye. The same region was imaged at two different times after intravenous injection of ICG dye (20 and 120 minutes, respectively), using different fields of view (0.75°, 1.0°, and 1.5°). There is a small region that was not imaged due to small differences in fixation and eye motion from one imaging session to another (*top left*, black box). The images were nearly identical, suggesting that the dye uptake is stable and can be imaged over at least 100 minutes. *Scale bar*: 50 μm.
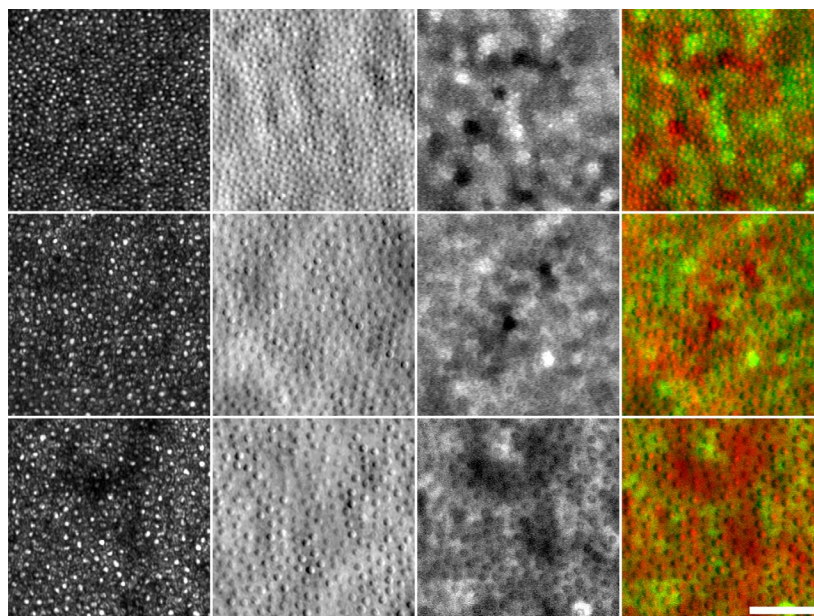
FIGURE 6. Simultaneous AOSLO imaging of multiple structures in the outer retina in subject HV2, left eye. Each row contains a set of simultaneously acquired images. (*Top* to *bottom*) Image acquired at a retinal location of 5°, 10°, and 15° in the temporal direction. (*Left* to *right*) Confocal reflectance, split detection, ICG, false color image (split detection, *red*; ICG, *green*) showing the imprinting effect of photoreceptors on the AO-ICG image. The cone photoreceptors are visible in confocal reflectance and split detection at all retinal eccentricities. Although individual RPE cells are visible at 5° temporal using both AO-ICG and AO darkfield, at larger eccentricities, the cell boundaries become more difficult to distinguish due to signal imprinting from the overlying photoreceptors. *Scale bar*: 100 μm.

may lead to a new clinical method to indirectly assess the health or status of the RPE layer as a whole using conventional methods for imaging ICG in the clinic, even without the use of AO technology. It should be noted that even though ICG undergoes rapid clearance from the blood plasma, the persistence of ICG in the RPE may reflect a longer time course for the clearance in cells that have internalized this fluorophore. Importantly, this persistence of ICG provides an extended period of time for AO imaging to occur, which is generally a lengthy process since a large number of overlapping images need to be acquired in order to reconstruct a larger montage. The ICG clearance time remains to be explored. In the future, implementation of real-time eye tracking capabilities,[20,39,40] in combination with streamlined imaging protocols, should lead to dramatic improvements in imaging throughput.

Adaptive optics-ICG complements existing AO techniques for imaging the RPE and has the added advantage that it uses near-infrared wavelength light for imaging, which is a safer alternative to visible sources of light due to the avoidance of photochemical damage associated with wavelengths of light shorter than 600 nm.[17] In addition, it does not rely on any intrinsic fluorophores such as lipofuscin, which varies with age and from person to person and which may be significantly altered in diseases such as age-related macular degeneration.[41,42] Instead, the use of an extrinsic fluorophore could provide a more objective way to probe the interface between the systemic circulation and RPE cells independent of unknown intrinsic signals. Because instrumentation for imaging ICG shares similarities with near-infrared autofluorescence (IRAF) instrumentation, the methods developed in this paper may contribute to future AO-enhanced IRAF imaging. However, this will require further improvements (Fig. 4A).

Future studies will also explore the potential use of AO-ICG for imaging the retinal and choroidal vasculature. Although OCT angiography[43-46] (including AO-based OCT angiography[47-50]) is becoming an attractive alternative to conventional

fluorescein and ICG angiography for vascular imaging, this does not preclude the use of AO-based angiography techniques such as AOSLO-based fluorescein angiography[24] when additional vascular detail is desired. It is also possible to use AOSLO-based angiography to obtain detailed images of the capillary
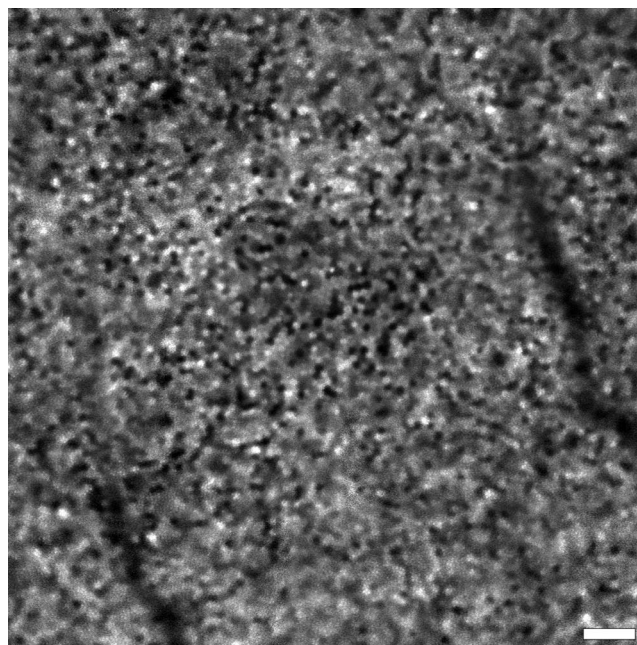

FIGURE 7. Adaptive optics-ICG image of RPE cells generated from 43 overlapping AO-ICG videos acquired in the late phase of ICG, at the fovea of subject HV2, right eye. Individual RPE cells appear to have relatively uniform fluorescence intensities. RPE cells can be visualized at various retinal eccentricities. Dark shadows from overlying blood vessels can be seen (*vertical lines* at the *upper right* and *lower left*). *Scale bar*: 100 μm.

network without the use of injected dyes,[51-53] to directly measure and track individual blood cells,[54-56] to measure pulsatility[54,57] and to assess vascular walls.[52,53] Application of AO-ICG to vascular imaging would further broaden the range of complementary approaches for assessing the vasculature for improving our understanding of disease.

In summary, AO-ICG provides a novel view of the RPE cell mosaic in the living human eye. The use of multimodal AO imaging will enable new investigations of relationships between photoreceptors and RPE cells in health and disease and will lead to valuable information about disease progression and the efficacy of current and future therapies for eye disease.

Acknowledgments

References

1. Desmettre T, Devoisselle JM, Mordon S. Fluorescence properties and metabolic features of indocyanine green (ICG) as related to angiography. *Surv Ophthalmol*. 2000;45:15–27.

2. Flower RW. Evolution of indocyanine green dye choroidal angiography. *Opt Eng*. 1995;34:727–736.

3. Mori K, Gehlbach PL, Nishiyama Y, Deguchi T, Yoneya S. The ultra-late phase of indocyanine green angiography for healthy subjects and patients with age-related macular degeneration. *Retina*. 2002;22:309–316.

4. Chang AA, Morse LS, Handa JT, et al. Histologic localization of indocyanine green dye in aging primate and human ocular tissues with clinical angiographic correlation. *Ophthalmology*. 1998;105:1060–1068.

5. Pankova N, Zhao X, Liang H, Baek DSH, Wang H, Boyd S. Delayed near-infrared analysis permits visualization of rodent retinal pigment epithelium layer *in vivo*. *J Biomed Opt*. 2014; 19:076007.

6. Liang J, Williams DR, Miller DT. Supernormal vision and high-resolution retinal imaging through adaptive optics. *J Am Opt Soc A*. 1997;14:2884–2892.

7. Roorda A, Romero-Borja F, Donnelly W II, Queener H, Hebert T, Campbell M. Adaptive optics scanning laser ophthalmoscopy. *Opt Express*. 2002;10:405–412.

8. Zhang Y, Poonja S, Roorda A. MEMS-based adaptive optics scanning laser ophthalmoscopy. *Opt Lett*. 2006;31:1268–1270.

9. Merino D, Duncan JL, Tiruveedhula P, Roorda A. Observation of cone and rod photoreceptors in normal subjects and patients using a new generation adaptive optics scanning laser ophthalmoscope. *Biomed Opt Express*. 2011;2:2189–2201.

10. Dubra A, Sulai Y. Reflective afocal broadband adaptive optics scanning ophthalmoscope. *Biomed Opt Express*. 2011;2: 1757–1768.

11. Zhang J, Yang Q, Saito K, Nozato K, Williams DR, Rossi EA. An adaptive optics imaging system designed for clinical use. *Biomed Opt Express*. 2015;6:2120–2137.

12. Liu Z, Kocaoglu OP, Turner TL, Miller DT. Imaging human retinal pigment epithelium cells using adaptive optics optical coherence tomography. *Proc SPIE*. 2016;96931E.

13. Torti C, Považay B, Hofer B, et al. Adaptive optics optical coherence tomography at 120,000 depth scans/s for non-invasive cellular phenotyping of the living human retina. *Opt Express*. 2009;17:19382–19400.

14. Felberer F, Kroisamer J-S, Baumann B, et al. Adaptive optics SLO/OCT for 3D imaging of human photoreceptors in vivo. *Biomed Opt Express*. 2014;5:439–456.

15. Roorda A, Zhang Y, Duncan JL. High-resolution in vivo imaging of the RPE mosaic in eyes with retinal disease. *Invest Ophthalmol Vis Sci*. 2007;48:2297–2303.

16. Morgan JIW, Dubra A, Wolfe R, Merigan WH, Williams DR. In vivo autofluorescence imaging of the human and macaque retinal pigment epithelial cell mosaic. *Invest Ophthalmol Vis Sci*. 2008;50:1350–1359.

17. Morgan JIW, Hunter JJ, Masella B, et al. Light-induced retinal changes observed with high-resolution autofluorescence imaging of the retinal pigment epithelium. *Invest Ophthalmol Vis Sci*. 2008;49:3715–3729.

18. Cideciyan AV, Jacobson SG, Aleman TS, et al. In vivo dynamics of retinal injury and repair in the rhodopsin mutant dog model of human retinitis pigmentosa. *Proc Natl Acad Sci U S A*. 2005; 102:5233–5238.

19. Rossi EA, Rangel-Fonseca P, Parkins K, et al. In vivo imaging of retinal pigment epithelium cells in age related macular degeneration. *Biomed Opt Express*. 2013;4:2527–2539.

20. Yang Q, Zhang J, Nozato K, et al. Closed-loop optical stabilization and digital image registration in adaptive optics scanning light ophthalmoscopy. *Biomed Opt Express*. 2014;5: 3174–3191.

21. Sharma R, Williams DR, Palczewska G, Palczewski K, Hunter JJ. Two-photon autofluorescence imaging reveals cellular structures throughout the retina of the living primate eye. *Invest Ophthalmol Vis Sci*. 2016;57:632–646.

22. Scoles D, Sulai YN, Dubra A. In vivo dark-field imaging of the retinal pigment epithelium cell mosaic. *Biomed Opt Express*. 2013;4:1710–1723.

23. Scoles D, Gray DC, Hunter JJ, et al. In-vivo imaging of retinal nerve fiber layer vasculature: imaging - histology comparison. *BMC Ophthalmol*. 2009;9:9.

24. Pinhas A, Dubow M, Shah N, et al. In vivo imaging of human retinal microvasculature using adaptive optics scanning light ophthalmoscope fluorescein angiography. *Biomed Opt Express*. 2013;4:1305–1317.

25. Scoles D, Sulai YN, Langlo CS, et al. In vivo imaging of human cone photoreceptor inner segments. *Invest Ophthalmol Vis Sci*. 2014;55:4244–4251.

26. Laser Institute of America. *ANSI Z136.1—Safe Use of Lasers* (2014). Orlando, FL: Laser Institute of America; 2014.

27. Dubra A, Harvey Z. Registration of 2D images from fast scanning ophthalmic instruments. In: Fischer B, Dawant BM, Lorenz C, eds. *Biomedical Image Registration. Lecture Notes in Computer Science*. Berlin: Springer; 2010:60–71.

28. Aurenhammer F. Voronoi diagrams—a survey of a fundamental geometric data structure. *ACM Computing Surveys*. 1991;23: 345–405.

29. Ach T, Huisingh C, McGwin G, et al. Quantitative autofluorescence and cell density maps of the human retinal pigment epithelium. *Invest Ophthalmol Vis Sci*. 2014;55:4832–4841.

30. Zonios G, Dimou A, Bassukas I, Galaris D, Tsolakidis A, Kaxiras E. Melanin absorption spectroscopy: new method for nonin-

vasive skin investigation and melanoma detection. *J Biomed Opt*. 2008;13:014017.

31. Burke JM. Mosaicism of the retinal pigment epithelium: seeing the small picture. *Mol Interv*. 2005;5:241–249.

32. Cideciyan AV, Swider M, Jacobson SG. Autofluorescence imaging with near-infrared excitation: normalization by reflectance to reduce signal from choroidal fluorophores. *Invest Ophthalmol Vis Sci*. 2015;56:3393–3406.

33. Keilhauer CN, Delori FC. Near-infrared autofluorescence imaging of the fundus: visualization of ocular melanin. *Invest Ophthalmol Vis Sci*. 2006;47:3556–3564.

34. Roorda A, Williams DR. Optical fiber properties of individual human cones. *J Vis*. 2002;2(5):404–412.

35. Benya R, Quintana J, Brundage B. Adverse reactions to indocyanine green: a case report and a review of the literature. *Cathet Cardiovasc Diagn*. 1989;17:231–233.

36. Hope-Ross M, Yannuzzi LA, Gragoudas ES, et al. Adverse reactions due to indocyanine green. *Ophthalmology*. 1994; 101:529–533.

37. Staller BJ. Adverse reactions after administration of indocyanine green. *JAMA*. 1978;240:635.

38. Yannuzzi LA. Indocyanine green angiography: a perspective on use in the clinical setting. *Am J Ophthalmol*. 2011;151:745–751.e1.

39. Arathorn DW, Yang Q, Vogel CR, Zhang Y, Tiruveedhula P, Roorda A. Retinally stabilized cone-targeted stimulus delivery. *Opt Express*. 2007;15:13731–13744.

40. Yang Q, Arathorn DW, Tiruveedhula P, Vogel CR, Roorda A. Design of an integrated hardware interface for AOSLO image capture and cone-targeted stimulus delivery. *Opt Express*. 2010;18:17841–17858.

41. Rudolf M, Vogt SD, Curcio CA, et al. Histologic basis of variations in retinal pigment epithelium autofluorescence in eyes with geographic atrophy. *Ophthalmology*. 2013;120:821–828.

42. Ach T, Tolstik E, Messinger JD, Zarubina AV, Heintzmann R, Curcio CA. Lipofuscin redistribution and loss accompanied by cytoskeletal stress in retinal pigment epithelium of eyes with age-related macular degeneration. *Invest Ophthalmol Vis Sci*. 2015;56:3242–3252.

43. Kim DY, Fingler J, Werner JS, Schwartz DM, Fraser SE, Zawadzki RJ. In vivo volumetric imaging of human retinal circulation with phase-variance optical coherence tomography. *Biomed Opt Express*. 2011;2:1504–1513.

44. Choi W, Mohler KJ, Potsaid B, et al. Choriocapillaris and choroidal microvasculature imaging with ultrahigh speed. *PLoS One*. 2013;8:e81499.

45. Braaf B, Vienola KV, Sheehy CK, et al. Real-time eye motion correction in phase-resolved OCT angiography with tracking SLO. *Biomed Opt Express*. 2013;4:51–65.

46. Jia Y, Tan O, Tokayer J, et al. Split-spectrum amplitude-decorrelation angiography with optical coherence tomography. *Opt Express*. 2012;20:4710–4725.

47. Hammer DX, Iftimia NV, Ferguson RD, et al. Foveal fine structure in retinopathy of prematurity: an adaptive optics fourier domain optical coherence tomography study. *Invest Ophthalmol Vis Sci*. 2008;49:2061–2670.

48. Zawadzki RJ, Choi SS, Fuller AR, Evans JW, Hamann B, Werner JS. Cellular resolution volumetric in vivo retinal imaging with adaptive optics–optical coherence tomography. *Opt Express*. 2009;17:4084–4094.

49. Wang Q, Kocaoglu OP, Cense B, et al. Imaging retinal capillaries using ultrahigh-resolution optical coherence tomography and adaptive optics. *Invest Ophthalmol Vis Sci*. 2011;52:6292–6299.

50. Zawadzki RJ, Miller DT. Retinal AOOCT. In: Drexler W, Fujimoto JG, eds. *Optical Coherence Tomography*. Chamfort NC: Springer International Publishing; 2015;1849–1920.

51. Tam J, Martin JA, Roorda A. Noninvasive visualization and analysis of parafoveal capillaries in humans. *Invest Ophthalmol Vis Sci*. 2010;51:1691–1698.

52. Sulai YN, Scoles D, Harvey Z, Dubra A. Visualization of retinal vascular structure and perfusion with a nonconfocal adaptive optics scanning light ophthalmoscope. *J Am Opt Soc A*. 2014; 31:569.

53. Chui TYP, VanNasdale DA, Burns SA. The use of forward scatter to improve retinal vascular imaging with an adaptive optics scanning laser ophthalmoscope. *Biomed Opt Express*. 2012;3:2537–2549.

54. Tam J, Tiruveedhula P, Roorda A. Characterization of single-file flow through human retinal parafoveal capillaries using an adaptive optics scanning laser ophthalmoscope. *Biomed Opt Express*. 2011;2:781–793.

55. Tam J, Roorda A. Speed quantification and tracking of moving objects in adaptive optics scanning laser ophthalmoscopy. *J Biomed Opt*. 2011;16:036002.

56. Bedggood P, Metha A. Direct visualization and characterization of erythrocyte flow in human retinal capillaries. *Biomed Opt Express*. 2012;3:3264–3277.

57. Zhong Z, Petrig BL, Qi X, Burns SA. In vivo measurement of erythrocyte velocity and retinal blood flow using adaptive optics scanning laser ophthalmoscopy. *Opt Express*. 2008;16:12746–12756.